DOI: 10.13009/EUCASS2022-4932
9TH EUROPEAN CONFERENCE FOR AERONAUTICS AND SPACE SCIENCES (EUCASS)

Combustion Characterization of LMP-103S in Strand Burner Experiments

James C. Thomas, Felix A. Rodriguez, David S. Teitge, and Eric L. Petersen
J. Mike Walker '66 Department of Mechanical Engineering, Texas A&M University
College Station, TX, 77845, Unites States

Abstract

LMP-103S is a storable, green, ammonium dinitramide (ADN)-based liquid monopropellant with significant potential owing to its improved specific impulse (≥ 6%) and density (∼24%) in comparison to hydrazine, and its superior safety and handling characteristics. LMP-103S already has a significant flight heritage but its baseline combustion behavior is a surprisingly understudied topic. Constant-volume strand burner experiments with LMP-103S are reported herein for pressures between 0.69 and 34.5 MPa (100 – 5,000 psia). Linear burning rates were measured from transient pressure data and high-speed video. Phenomenological combustion behaviors are reported for the entire pressure range as deduced from these diagnostics.

1. Introduction

Hydrazine has been the liquid monopropellant of choice for space propulsion applications for over half a century due its high performance, clean exhaust products, and heritage knowledge base. However, high operational deployment costs and toxicity concerns have driven the search for a 'green' replacement that has higher performance, low toxicity, and is more environmentally friendly. Global programs aimed at hydrazine replacement have included the NASA green propellant infusion mission (GPIM) project and the EU green advanced space propulsion (GRASP), pulsed chemical rocket with green high-performance propellants (PulCheR), and replacement of hydrazine for orbital and launcher propulsion systems (RHEFORM) projects. A recent review of state-of-the-art green monopropellants for propulsion is provided by Nosseir et al. [1]. In general, green monopropellants can be categorized as: 1) energetic ionic liquids (EILs), 2) liquid NOx monopropellants, or 3) aqueous hydrogen peroxide solutions (HTP).

In general, EILs consist of oxidizer salts dissolved in aqueous solutions mixed with fuel components. Oxidizers that have been more widely studied for use in EILs include hydroxylammonium nitrate (HAN) and ammonium dinitramide (ADN), amongst others, while a wide variety of molecular and ionic fuels have been considered. LMP-103S is an ADN-based liquid monopropellant developed by Bradford ECAPS consisting of 63.0% ADN, 18.4% methanol, and an 18.6% balance solution of water/ammonia (75/25) [1]. In comparison to alternative EILs, LMP-103S has extensive flight heritage through the PRISMA and SkySat missions, and ECAPS now offers a range of thrusters (0.1-220 N) that operate with LMP-103S [2]. In addition, LMP-103S touts a theoretical specific impulse of ∼252 s and a standard density of 1.25 g/cm^3 [3], yielding performance increases over hydrazine of ≥ 6% and ∼24% for specific impulse and density, respectively. However, direct comparison of delivered performance during the PRISMA mission indicated LMP-103S provided up to 20% higher specific impulse than hydrazine, depending on thruster operation mode [3-4].

Despite a significant body of research surrounding LMP-103S development and characterization, and a proven history of successful flight heritage, the fundamental combustion properties of this liquid monopropellant are understudied and relevant data are lacking in the literature. This work explores the fundamental combustion behavior of LMP-103S with an optically accessible strand burner experiment. The following section provides an overview of the experimental methods employed herein. Linear burning rates and phenomenological combustion observations from these experiments are subsequently discussed. Finally, key findings are summarized in the Conclusion section.

2. Experimental Methods

LMP-103S monopropellant was provided by ECAPS and utilized as-received. Combustion properties of liquid propellant samples were evaluated with an optically accessible strand burner. A detailed description of the strand

DOI: 10.13009/EUCASS2022-4932

burner apparatus employed herein is given by Warren [5] and experimental procedures have been previously described by McCown et al. [6] and Thomas et al. [7]. The experimental apparatus and methodology are briefly described herein for completeness, as follows. Combustion experiments were performed in a closed-volume, static strand burner (Fig. 1) consisting of a cylindrical test chamber, four optical ports, and several diagnostics including a spectrometer, photodiode, high-speed camera, and pressure transducers. Liquid propellant is loaded into a quartz tube (7 x 30 mm) and then into the burner plug (Fig. 1); a Nichrome wire coil is attached to the plug electrodes and submerged within the liquid propellant just below the surface; and the burner plug is loaded into the strand burner. Inert gas (N_2 or Ar) is utilized to slowly pressurize the system to the desired test pressure. Ignition is achieved by passing a low-amperage electrical current (3.5 A, 6 V) through the Nichrome wire until sufficient pre-heating has taken place to yield propellant ignition.

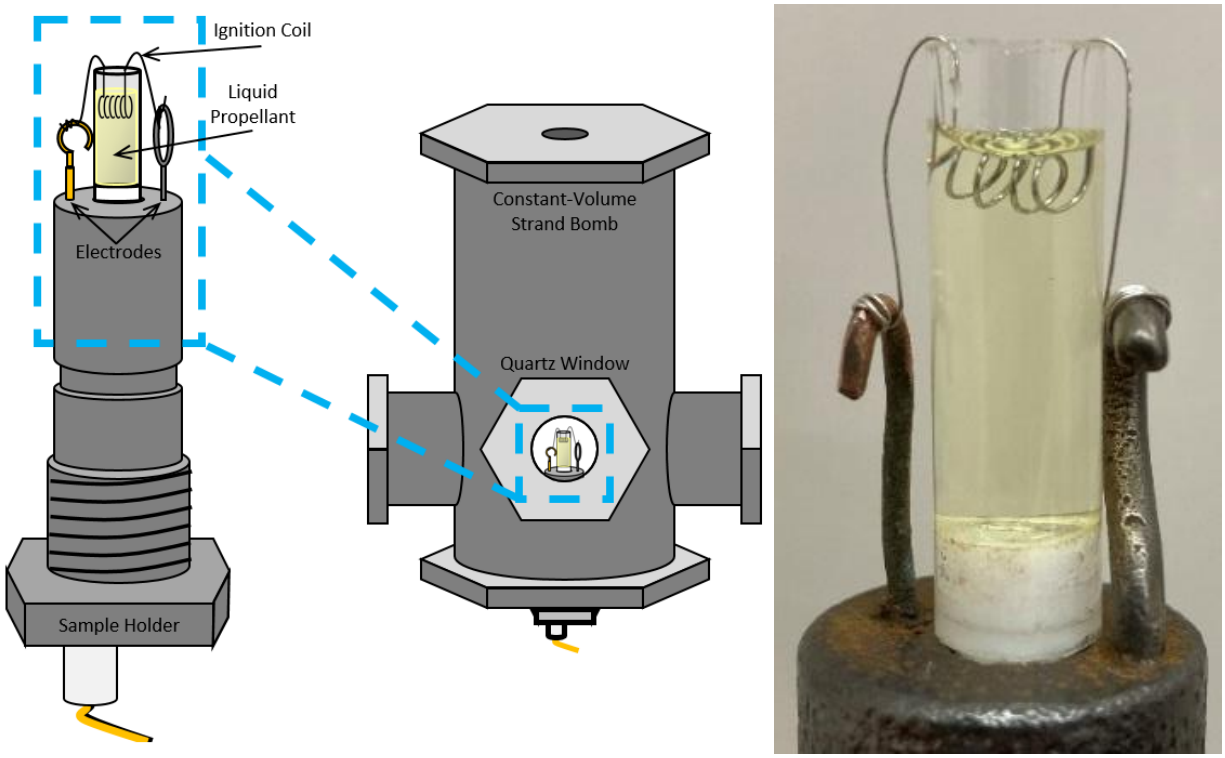

Figure 1: (left) Schematic representation of the strand burner and liquid propellant mount. (right) Image of an LMP-103S sample prepared for strand burner testing.

Propellant ignition and combustion processes are visually monitored with high-speed video and are described qualitatively in the following section. Quantitative measurements include the ignition delay time and burning rate of the propellant. The propellant ignition delay time is defined as the time between initial application of electrical current to the propellant until the first appearance of sustained propellant combustion. The propellant burning rate is calculated from high-speed video tracking analysis of the gas-liquid interface and by means of the pressure transducer data trace. The propellant burning rate is given by:

$$r = \frac{\Delta H}{t_b} = \frac{4m}{\pi \rho t_b d^2} \quad \textbf{(1)}$$

where ΔH is the change in height of the propellant column, t_b is the burn time of the propellant, m is the mass of propellant burned, ρ is the propellant density, and d is the inner diameter of the quartz tube (7 mm). In the video-based method, the change in propellant height is manually tracked via imaging analysis software, and the burn time is given by the time between video frames and the total number of frames covering the burning process. In the pressure-based method, the burn time is measured from the pressure transducer data trace of the combustion event. Care should be taken in selecting the end point of propellant combustion when utilizing the pressure-based method due to the two-phase decomposition behavior of some ionic liquid monopropellants, as further described by Thomas et al. [7]. Ignition delay times were measured manually with a stopwatch.

DOI: 10.13009/EUCASS2022-4932

3. Results and Discussion

Optically measured burning rates and ignition delay times for LMP-103S burning in inert (N_2 or Ar) environments are shown in the left and right plots of Fig. 2, respectively. In general, no differences are observed for measurements between the two different inert gases. Two pressure regimes are observed within the data, termed the low- and high-pressure regimes herein. In the low-pressure regime (P < 9.5 MPa), the burning rate increases with pressure and is well-represented by a power law:

$$r = 2.11 \times 10^{-2}\, P^{2.99} \quad \textbf{(2)}$$

where the units for burning rate and pressure are mm/s and MPa, respectively. The ignition delay time decreases modestly with increasing pressure in this regime. The low-pressure deflagration limit (LPDL) measured herein was approximately 3.5 MPa. In the high-pressure regime, the burning rate continues to increase with pressure and can be represented by an off-set power law:

$$r = -391 + 59.8\, P^{0.88} \quad \textbf{(3)}$$

The ignition delay time sharply decreases at the onset of the high-pressure regime (~ 8.3 MPa) and rapidly approaches the experimental measurement error (~ ±0.3 s) at a pressure of approximately 11 MPa. The burning rate data collected herein are compared to the only three data points available within the literature [8] and exhibit moderate agreement.

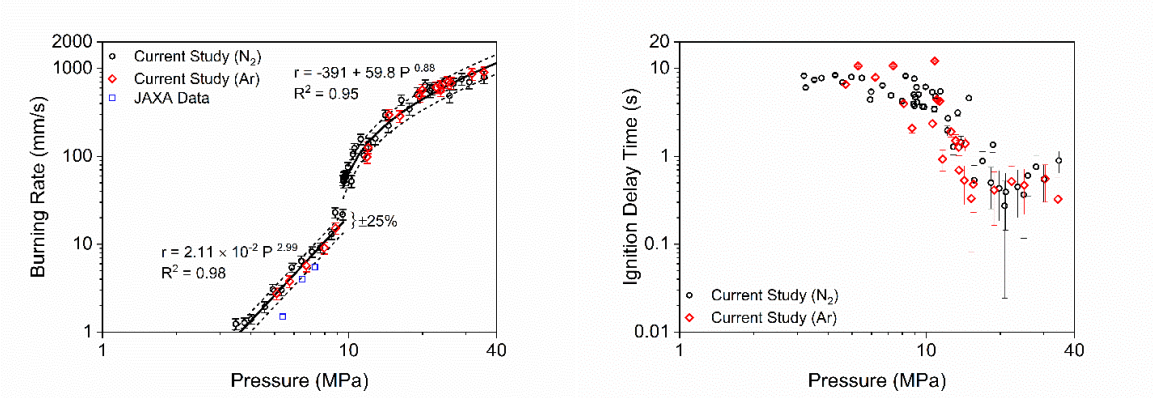

Figure 2: Optically measured (left) burning rates and (right) ignition delay times for LMP-103S burning in inert (N_2 or Ar) atmospheres.

Representative pressure and light emission data, and corresponding high-speed video still frames for an experiment in the low-pressure regime are shown in Fig. 3. Application of current to the ignition coil causes rapid combustion of the propellant surrounding the coil. A steady increase in pressure and decrease in liquid propellant column height are observed throughout the remaining duration of the experiment. The flame structure consists of a liquid propellant region, a two-phase zone, and a coupled visible flame region.

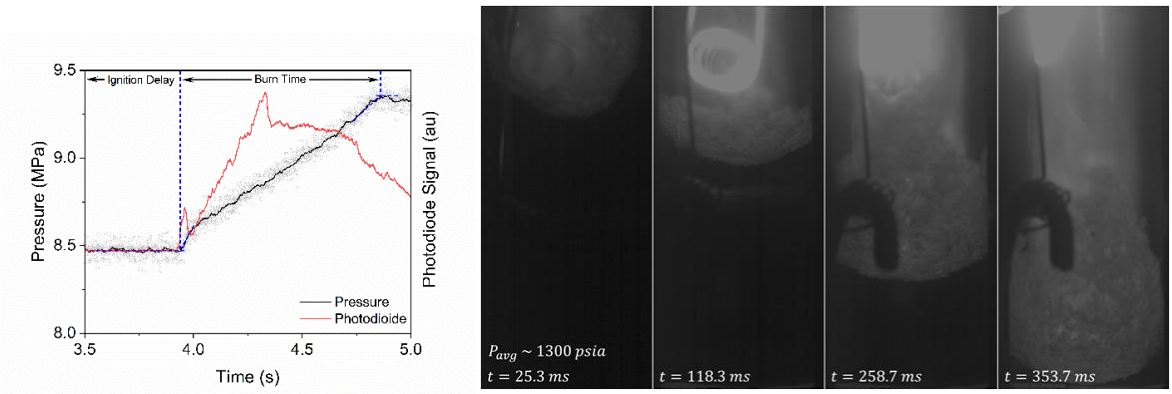

Figure 3: Representative pressure and light emission data, and high-speed video still frames from the combustion of LMP-103S in the low-pressure regime.

DOI: 10.13009/EUCASS2022-4932

Representative pressure and light emission data, and corresponding high-speed video still frames for an experiment in the high-pressure regime are shown in Fig. 4. Ignition of the propellant is immediately followed by a steady increase in pressure and decrease in liquid propellant column height. No significant light emission is noted from a flame while the liquid propellant regresses. After all the liquid propellant has decomposed and gasified, a visible flame rapidly propagates through the tube. The structure observed inside of the quartz tube is comprised of virgin propellant and a discrete gas/liquid interface at its regressing surface, until the final flame propagates through the tube.

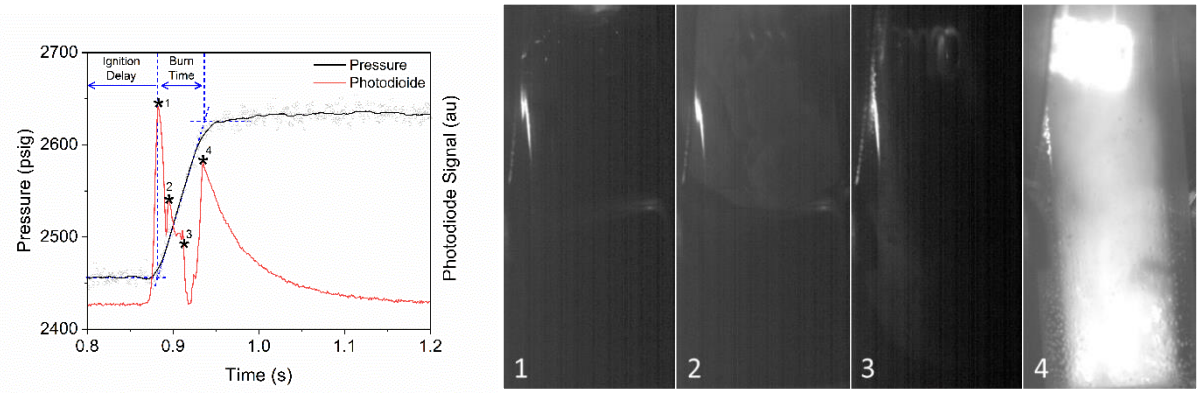

Figure 4: Representative pressure and light emission data, and high-speed video still frames from the combustion of LMP-103S in the high-pressure regime.

High-speed video still frames have been selected from the range of pressures evaluated herein and are shown in Fig. 5 to illustrate general qualitative behaviors observed during experiments. In addition, schematic representations of the pressure-dependent propellant combustion zones and flame behavior are shown in Fig. 6. In the low-pressure regime ($P < 8.3$ MPa), the gas/liquid interface is characterized by a thick, two-phase layer with a range of bubble sizes. The two-phase region is turbulent and rapid migration of bubbles is evident. In addition, larger bubbles were observed to 'pop' and release pockets of partially reacted decomposition gases. In many cases, bubbles are forced into the liquid propellant and pop therein, releasing hot gases below the gas/liquid interface and significantly increasing turbulence in this region. A visible flame attached to the gas/liquid interface was observed in all experiments within the low-pressure regime. Significant local flame luminosity fluctuations were observed and generally corresponded to popping events from larger bubbles. The average bubble size significantly decreases as the pressure is increased within the low-pressure regime

Small bubbles and a turbulent interface are observed above the critical transition pressure ($P \sim 8.3$ MPa) and up until a pressure of approximately 11 MPa. The interface gradually transitions from a two-phase region to a discrete turbulent interface over this pressure range (8.3 – 11 MPa), and no bubbles are observed at higher pressures. At pressures above 11 MPa, the gas/liquid interface develops cellular structures and the visible flame decouples from the regressing propellant surface. In general, high-speed videos taken above this pressure did not contain significant luminosity from a visible flame and secondary LED lighting was required for visualization of the surface. Once all the liquid propellant had been consumed, a visible flame rapidly propagated through the quartz tube (Fig. 4). The visible flame structure began to re-couple to the surface at the highest evaluated pressures herein (> 30 MPa), but only at the tips of regressing cells (see last frame of Fig. 5).

DOI: 10.13009/EUCASS2022-4932

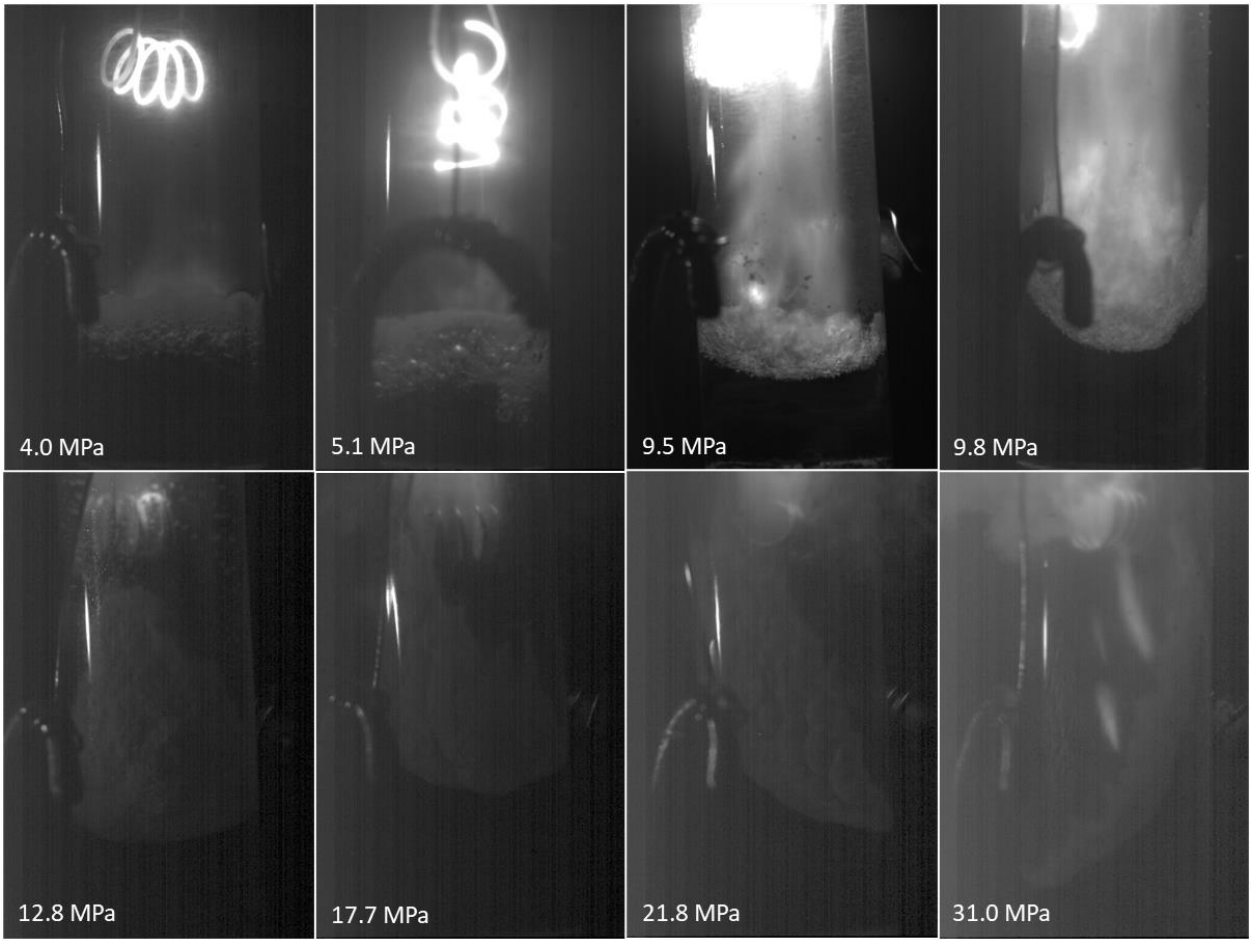

Figure 5: High-speed video still frames from experiments conducted over a wide range of pressures illustrating the change in combustion behavior.

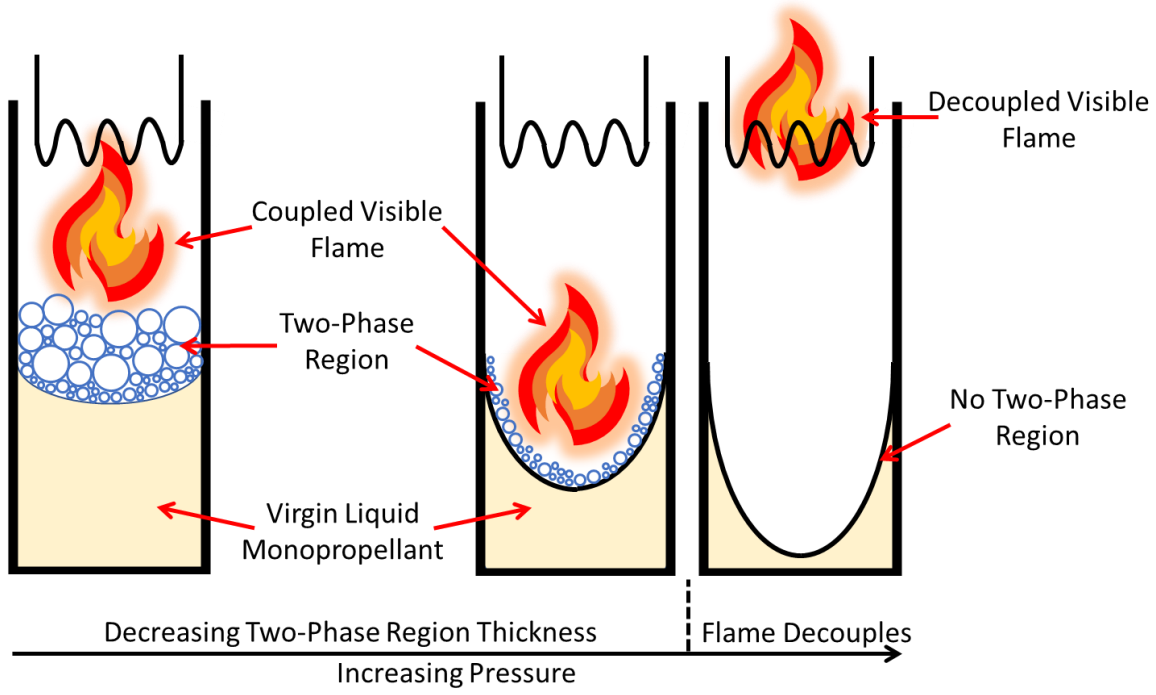

Figure 6: Schematic representation of the pressure-dependent propellant combustion zones and flame behavior.

DOI: 10.13009/EUCASS2022-4932

4. Conclusion

Two separate combustion regimes were observed during optically accessible strand burner experiments with LMP-103S. In the low-pressure regime (P < 9.5 MPa), hydrodynamic instabilities at the two-phase foam gas/liquid interface can transport hot, partially reacted gas bubbles into the cold liquid propellant, and a visible flame is coupled to the regressing propellant surface. As the pressure is increased, the thickness of the two-phase zone decreases and becomes discrete. Transition to the high-pressure regime at a critical pressure (P ~ 11 MPa) may be triggered by supercritical combustion conditions and causes the visible flame to become uncoupled from the regressing propellant surface. The burning rate data presented herein significantly extend the available data in the literature and provide unique insight into the combustion behavior of LMP-103S and similar ADN-based liquid monopropellants over a wide range of conditions.

References

[1] Nosseir, A. E. S., Cervone, A., and Pasini, A. 2021. Review of State-of-the-Art Green Monopropellants: For Propulsion Systems Analysts and Designers. *Aerosp*. 8:1-21.

[2] High Performance Green Propulsion <https://www.ecaps.space/hpgp-performance.php> Accessed March 8, 2022.

[3] Anflo, K., and Crowe, B. 2011. In-Space Demonstration of an ADN-based Propulsion System. *47th AIAA Joint Propulsion Conference*. AIAA 2011-5832.

[4] Persson, M., Anflo, K., Dinardi, A., and Bahu, J. M. 2012. A Family of Thrusters for ADN Based Monopropellant LMP 103S. *48th AIAA Joint Propulsion Conference*. AIAA 2012-3815.

[5] Warren, W. C. 2012. Experimental Techniques for the Study of Liquid Monopropellant Combustion, MS Thesis, Texas A&M University, College Station, TX, USA.

[6] McCown III, K. W., Demko, A. R., and Petersen, E. L. 2014. Experimental Techniques to Study the Linear Burning Rates of Heterogeneous Liquid Monopropellants. *J. Propuls. Power* 30:1027-1037.

[7] Thomas, J. C., Homan-Cruz, G. D., Stahl, J. M., and Petersen, E. L. 2019. The Effects of SiO2 and TiO2 on the Two-Phase Burning Behavior of Aqueous HAN Propellant. *Proc. Combust. Inst*. 37:3159-3166.

[8] Anflo, K., Thormahlen, P., and Persson, M. 2016. HPGP Monopropellant LMP-103S: Propellant Description and Test Summary. DOX-RBS-142634. ECAPS. Solna, Sweden.